33RD CONGRESS
OF THE INTERNATIONAL COUNCIL
OF THE AERONAUTICAL SCIENCES
STOCKHOLM, SWEDEN, 4-9 SEPTEMBER, 2022

ICAS 2022 SWEDEN

SERIES-HYBRID RETROFIT OF AN XV-15 TILTROTOR AND EMERGENCY PROCEDURE ENERGETIC ANALYSIS

Giulio Avanzini[1], Giovanni Bernardini[2], Simone Moretti[2] & Jacopo Serafini[2]

[1]Department of Engineering for Innovation, University of Salento, Via Monteroni, 73100, Lecce, Italy
[2]Department of Engineering, Roma Tre University, Via Vito Volterra 62, 00146, Roma, Italy

Abstract

This paper presents the main outcomes of a research activity aimed at defining a series-hybrid version of the tiltrotor XV-15 through a retrofit process of its power train. This research is motivated by the interest in electrification of aircraft propulsion and the concurrent envisaged rising of short-range air mobility services, which makes tiltrotors an appealing solution due to its capability of vertical take-off and the possibility of alleviating several of its shortcomings through electrification. Indeed, in a Internal Combustion Engine tiltrotor, both engines must be capable to generate the power required to hover in case of one engine failure. This causes the need to mount engines heavier than needed. Moreover, the need to have null overall yawing moment imposes the presence of a shaft along the entire wing to transmit power. This shaft conditions the wing shape and structure, causing small efficiency and heavy weight. The proposed propulsive retrofit is based on a turboshaft/electric generator group powering the two electric motors, with a battery pack acting as a peaker for high-power phases like hovering and climb. During the low-power descent and loiter phases, the battery pack is recharged by the turboshaft. In order to optimize the battery weight, the pack is split into two: one is formed by Li Ion cells, which have high specific energy and the other is formed by Li-Po cells, which have higher specific power and lower specific energy. With the technology available today, the maximum take-off weight of the XV-15 cannot be either reduced or maintained with a simple propulsive retrofit, mainly due to battery weight. Considering a technological improvement similar to that experienced by batteries during last two decades, it is likely to reach a break even point in few years (<20). The presence of a battery pack onboard allows to have only one internal combustion engine with fewer safety issues in case of an engine failure. One of the remaining safety issues is the possible insurgence of engine failure when the batteries are at the lowest state of charge, e.g. after the initial climb in a typical mission profile. In the proposed emergency procedure, the aircraft rotors extract power from the flow during the gliding flight recharging the batteries, becoming able to conduct a fully-powered landing in helicopter mode, with an hovering time varying from 30 to 110 seconds, depending on the descent strategy.

Keywords: Series-Hybrid propulsion, tiltrotor, emergency landing

1. Introduction

Since the introduction of jet engines, air transport has undergone considerable development, doubling its volume approximately every 20 years [23]. For this reason, its environmental impact, especially in terms of polluting emissions and noise, has gained more and more attention. Switching to electric propulsion in the next decades is considered as the most promising way to decrease the impact on the environment of the aviation sector, as demonstrated by a growing interest from manufacturers, regulatory offices and aviation community. [11, 19, 25, 32, 31]

However, despite their quick improvements (about 8%/year for specific energy), batteries and fuel cells are not yet able to guarantee the required performance [3, 24, 39, 27, 36, 20, 9, 10] As an intermediate, short-term step, the hybrid electric propulsion (as proposed by AIRBUS in the E-FAN X project [30]) promises several benefits [4, 22]: a significant decrease of pollutants and greenhouse

gases emissions, the reduction of noise, an overall increase in flight operations safety thanks to the superior reliability of the electric elements, as well as the design flexibility enabled by distributed propulsion and very high acceleration capabilities.
At present, land transport is still far more convenient for regional and inter-city transport, as long as airports require large spaces and must be often located far from urban centers due to noise impact. Hybrid electric (and - further in the future - fully electric) propulsion can mitigate this problem, connecting centers poorly connected by road and rail infrastructures with point-to-point routes. Furthermore, the use of Vertical Takeoff and Landing (VTOL) aircraft require vertiports which are much less soil-consuming than airports.
Tiltrotors combine the VTOL and hover flight capabilities of helicopters, with performance in terms of speed, range, endurance, and ceiling altitude approaching those of conventional turboprops.
As far as the application of Civil Tiltrotors in the framework of commercial transport is concerned, this class of aircraft is expected to alleviate the congestion of major airport hubs, reducing at the same time delays, while increasing passenger throughput capacity [37, 40], thanks to their ability to conduct Runway Independent Operations (RIO) [5].
However, Reference [37] shows that a future fleet of these class of aircraft would have an impact in terms of fuel consumption (and therefore polluting emissions) and acoustic impact comparable with that of a fleet of traditional fixed-wing aircraft. Therefore, the use of electric or hybrid electric propulsion for this category of aircraft is fundamental for their future use.
Moreover, the advantages of this type of propulsion systems go beyond the abatement of emissions and noise. An interesting advantage lies in the possibility of eliminating the complex mechanical transmission that connects the two turboshaft engines in order to guarantee operations in One Engine Inoperative (OEI) condition. This system has implications on the wing structure of tiltrotors which notoriously has a reduced span and a high thickness, the latter of the order of 20% of the chord, leading to an obvious increase of drag. Electric or hybrid electric propulsion allows to totally eliminate this complex transmission system by replacing it with a system of redundant cables that guarantee the continuous power supply of the electric motors [6].
Considering series-hybrid aircraft, the most likely propulsion fault is the internal combustion engine failure. Although these aircraft are inherently safer than traditional ones due to the presence of batteries that can power an emergency landing, at some point during flight the batteries reach the minimum state of charge. In the case of a failure at that point, the hybrid aircraft is forced to glide and then land. However, also in this case, the presence of a battery pack on-board of the aircraft still increases the safety of the emergency procedure, if the decelerated descent is used to recharge the batteries, gaining the possibility to perform an electrically powered emergency landing in helicopter mode.
Some examples of hybridization of tiltrotor aircraft can be found in the literature, as in the case of Reference [14] which proposes the concept of a 6-seater tiltrotor, on which it is possible to integrate two different hybrid propulsion systems (differently sized) or a completely electric propulsion system, consequently varying the characteristics of speed, range and ceiling altitude of the aircraft. Finally, in reference [6] NASA proposes the hybrid electric retrofit of the Bell XV-15 using a parallel hybrid electric propulsion system integrating in each engine nacelle both the turboshaft engine and five electric motors connected in series. This study demonstrates how the retrofit operation leads to a reduction in consumption of 10% at the cost of an increase in the empty weight of the aircraft by 25% (still considered acceptable).
This work proposes a conceptual retrofit of a Bell XV-15 tiltrotor aircraft with hybrid electric propulsion, with the aim of sizing a substitute of the powertrain of the XV-15 with a series hybrid architecture, exploiting the wide literature data for this aircraft. The definition of the mission profile is followed by the evaluation of the power required, which is necessary for sizing the internal combustion engine and batteries. Once the power split is defined, the elements of the propulsion system are sized, taking into account current and future technological levels. The retrofit process provides a balance between the weights of the new propulsion system and those eliminated from the original configuration owing to the new propulsion system, to assess the feasibility and the impact that the conversion to electric hybrid propulsion has on the tiltrotor Design Take Off Weight (DTOW). This is intended to verify if the

calculated power levels with the current technological level guarantee the proposed retrofit operation or if it is necessary to wait for future technological developments. Furthermore, the capability of the XV-15 to perform a regenerative emergency descent in case of engine failure is assessed, to evaluate the eventual increase of safety of a hybrid tiltrotor performing landing in helicopter mode powered by batteries.

2. Retrofit process

2.1 Selection of the propulsion system

A series-hybrid electric propulsion system has been chosen for the XV-15 retrofit operation, being the most suited for multi-propeller aircraft and therefore also for the twin-rotor configuration of a tiltrotor. This configuration has the advantage of removing the turboshaft engines from the nacelles, allowing to eliminate all the problems related to their operation when they are tilted (e.g. lubrication). This allows also the nacelle lightening as the electric motors are lighter than turboshafts, as well as the elimination of the mechanical transmission passing through the wing, with the related possible improvements on the wing structure and aerodynamics. The propulsion system proposed in this work is sketched in fig. 1.

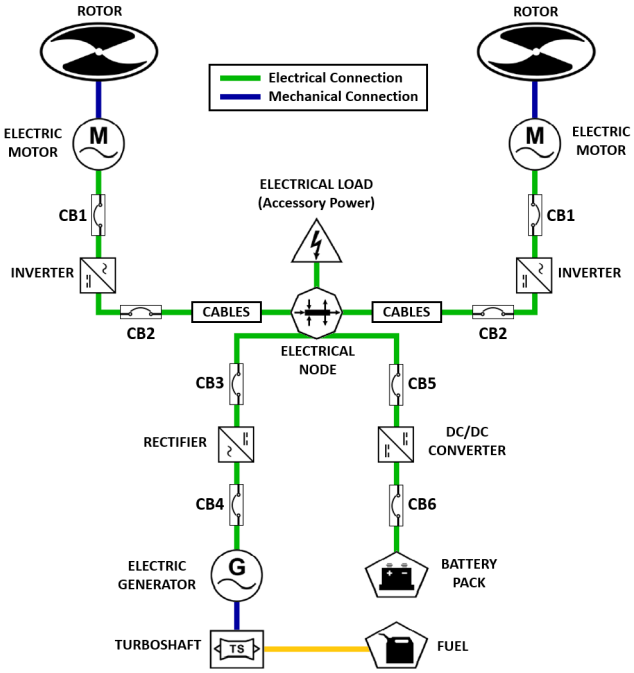

Figure 1 – Scheme of the propulsion system considered for the retrofit operation

The selected system consists of five branches which are connected through an electrical node: **(i) the PGS branch**, which includes the Power Generation System (PGS) consisting of the turboshaft engine, the electric generator and the AC/DC rectifier; **(ii) the battery branch**, which extends from the battery pack to the electrical node thus also including the DC/DC converter to control the voltage supplied by the batteries; **(iii) two rotor branches**, that are two identical branches extending from the electrical node to the aircraft rotors (these include the cables system and the DC/AC inverters); **(iv) the accessory branch**, which represents the connection between the electrical node and the on-board systems of the aircraft (not described in detail, whose presence is taken into account through the required accessory power).
The propulsion system is sized considering the PGS capable of delivering the power for the cruise flight and the onboard systems. For the remaining flight phases (climbs and HM phases), it is also required to consider the power supplied by the batteries.

2.2 Mission profile

The choice of the mission profile represents the first fundamental step in the preliminary design/retrofit process of an aircraft. For tiltrotor configurations, it allows identifying the flight phases in helicopter

and aircraft modes and evaluating the power and energy required by these phases to proceed with the sizing of the propulsion system.
In this work, with the aim of considering a typical mission of the XV-15, the mission indicated in [17] is chosen. The mission provides the following phases: (1) vertical take off followed by a hovering/vertical climb and a conversion phase from HM to AM; (2) climb to the cruise altitude of $20000\,\mathrm{ft}$; (3) first half of the cruise segment; (4) descent to an altitude of $10000\,\mathrm{ft}$; (5) loiter at best endurance speed ($\mathrm{V_{BE}}$); (6) climb to cruise altitude; (7) second half of the cruise segment; (8) descent to sea level; (9) vertical landing preceded by a conversion phase from AM to HM and a hovering phase.
In addition to the loiter phase between two cruise segments, in accordance with the regulations, it is necessary to consider a further loiter phase during the final descent for emergency reasons (e.g., related to particular air traffic or meteorological conditions) or alternatively the continuation of the flight to an alternate airport. Therefore, following the EASA regulations [34] for helicopters (as tiltrotors are considered to belong to the rotorcraft family), an additional fuel quantity for flying 20 or 30 minutes, respectively for VFR or IFR flight rules, are considered. In this work, the retrofit process is based on the worst case, adding to the mission profile of a loiter phase lasting 30 minutes at the same altitude as the previous loiter phase. In the following, this loiter phase will be called “extra loiter" to distinguish it from the previous one.

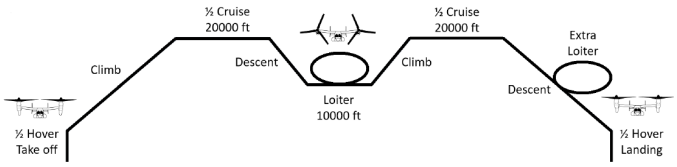

Figure 2 – Mission Profile

The duration of the mission profile phases is defined by following [17], that allows the selection of the times of each of the phases of the XV-15 mission. In this paper, the mission which maximizes the overall cruising time is considered. Table 1 summarizes the time scheduling of all the mission profile phases, also indicating the corresponding ranges. Note that the two phases of HM are considered equal to half the total hover time, and the final descent is divided into two segments of equal duration with the extra loiter placed between them.

Table 1 – Mission phases Endurance and Range

Mission segment	Endurance [min]	Range [km]
HM #1	3	-
Cruise Climb	7	58.2
Cruise #1	20.55	192.8
Loiter Descent	2.8	26.2
Loiter	18	-
Loiter Climb	3.5	29.1
Cruise #2	20.55	192.8
Descent #1	2.8	26.2
Extra Loiter	30	-
Descent #2	2.8	26.2
HM #2	3	-
Total mission	114	551.9

Furthermore, the two conversion phases have been embedded in the HM phases, as the single conversion requires a total time slightly above 10 seconds (time estimated knowing that the XV-15 has an angular velocity of the nacelles equal to 7.5°/s [7] and that a total rotation of 90° is performed during the conversion).

2.3 Required Power Evaluation

Once the mission profile is defined, the required power for each mission phase is evaluated and shown in Figure 3 (to better identify the different mission phases, the mission profile is also depicted).

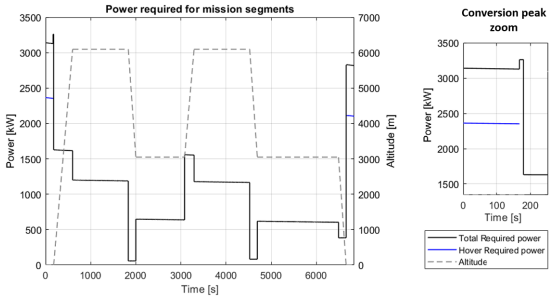

Figure 3 – Aircraft total power trend

This figure shows that the helicopter mode phases are those with the highest power demand, followed by the two climb phases in airplane mode. The minimum power is required during the descent phases, and the maximum power peak (although of short duration) is required for the conversion phase from HM to AM (a zoom of this peak is also shown in Figure 3 for clarity). Furthermore, note that the HM phases also include the conversion power.

For a correct interpretation of the previous graph, it is paramount to consider the propulsive system power flows. Indeed, the propulsion system has an electrical node with input powers from the PGS and the batteries, and accessory (necessary for the onboard systems of the aircraft) and propulsive (sent to the two rotors) powers as output powers. Therefore, the electrical node is characterized by the following balance equation

$$\mathrm{P_{PGS}} + \mathrm{P_{BAT}} = \mathrm{P_{ACC}} + 2\,\mathrm{P_{PROP}} \tag{1}$$

where the accessory power has been assumed to be constant and estimated by following [6] as $\mathrm{P_{ACC}} = 49.2\,\mathrm{kW}$. Furthermore, the power indicated as $\mathrm{P_{PROP}}$ represents the power at the "rotor level" ($\mathrm{P_{rotor}}$) increased for the "branch efficiency", that is the efficiency of all the elements between the rotor and the electrical node.

2.4 Specific Fuel Consumption

Since the aircraft considered in this work has a hybrid electric propulsion system, it will be affected, similarly to conventional propulsion aircraft, by a gradual weight loss due to fuel consumption. The estimation of the Specific Fuel Consumption (SFC) related to the different mission phases is required to take into account the weight loss in the evaluation of the corresponding necessary powers. In this paper, an SFC value is defined for each mission segment, using the regression model proposed in [28]. This model is based upon the SFC values of several existing turboshaft engines and allows expressing the SFC as a function of the engine size and three variables: altitude, forward speed, and partial load.

2.5 In-flight battery charging

The serial hybrid electric propulsion system allows the recharge of batteries during the flight phases in which they are not directly used, simply exploiting the surplus of power coming from the PGS, ensuring that the turboshaft engine supplies power to the generator shaft greater than that strictly necessary for the propulsion and on-board systems of the aircraft.

In this work, the need to recharge the batteries during the flight comes from the choices made on the division of power between the PGS and the batteries and the considered mission profile. Indeed, the starting point of the first cruise segment represents an energetically critical point of the mission in which the batteries are completely discharged from the previous phases of vertical take-off, conversion, and climb. Furthermore, being the PGS sized to have the cruising power as maximum power, it is paramount to recharge the batteries to have the power and energy necessary for the remaining climb and helicopter mode phases. This requires managing the power supplied by the PGS in the flight phases that do not involve the use of batteries to be able to recover energy to be stored, The

energy balance depicted in fig. 4 shows the trend of both the necessary power (black line) and the power supplied by the PGS (red dotted line), the latter managed in such a way to guarantee the balance between the blue areas, representing the recharged energy, and the green areas, representing the energy supplied by the batteries in the phases where they are needed.

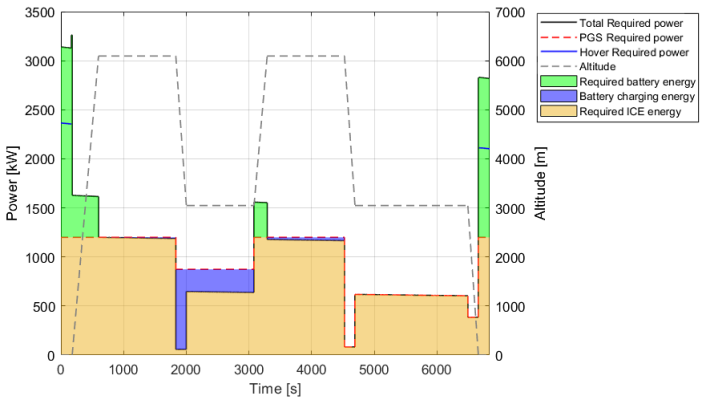

Figure 4 – Power and energy trend

Namely, during the phases of the cruise, loiter and descent preceding the loiter, the PGS supplies an excess of power to guarantee the recharging of the batteries. Indeed, during cruise phases, the maximum power level is always maintained, regardless of whether the power needed to fly is less due to the aircraft weight reduction. A similar strategy is used during the other two phases (loiter and descent to lioter), although a power value lower than the maximum one is maintained. The last phases of the mission are excluded from the recharging scheduling because the recharge at the end of the second cruise segment provides enough energy to complete the mission (without having to recharge batteries in the final descent).

3. Propulsion system sizing

3.1 Sizing methodology and power management

An approach based on the use of specific power is used for sizing the electric generator, electric motors and power converters, thus defining the mass of the generic element as follows:

$$\mathrm{M_e} = \mathrm{P_{out}}/\mathrm{p_e} \tag{2}$$

where $\mathrm{M_e}$ indicates the element mass, $\mathrm{p_e}$ the specific power of the element [kW/kg] while $\mathrm{P_{out}}$ represents the power provided by the element. Specifically, for the generic element, the output power is defined as the output power of the previous element suitably increased by its efficiency (see eq. (3)).

$$\mathrm{P_{out2}} = \mathrm{P_{out1}}/\eta_1 \tag{3}$$

On the basis of the current technological level, table 2 summarizes the values of the efficiencies used in the propulsive system sizing.

Table 2 – Propulsion System Elements Efficiency

Elements	Efficiency
Electric Motor/Generator	98%
Power Converters	99%
Cables	98%
Circuit Breakers	99%

Still maintaining the same methodology for the evaluation of powers, the masses of the turboshaft engine and the circuit breakers are evaluated by using the approach proposed in [38] and [15]:

$$\mathrm{M_{gt}} = 0.9594\,\mathrm{k_{gt}}\,(\mathrm{P_{shaft,gt}})^{0.7976} \mathrm{M_{IGBT}} = (1.6\cdot 10^{-4}\,\mathrm{P_{IGBT}}) + 0.6 \tag{4}$$

In this equation, the mass of the turboshaft engine (M_{gt}) depends not only on the power but also on the parameter k_{gt}, which indicates a technological factor of the gas turbine that can be used to account for expected improvement in turbo machinery technology [38] (assumed in this work of unitary value). Furthermore, the mass of the circuit breakers (M_{IGBT}) refers to the so-called Solid State Power Controllers (SSPC), widely used in the aeronautical sector for high voltage and high power applications, which are usually realized through the use of IGBT (Insulated Gate Bipolar Transistor) [29].
Since the two branches of the propulsion system connecting the rotors to the electrical node manage the same amount of power (i.e., half of the total power required), it is necessary to size only one of them, then doubling the weights obtained. The sizing process considers that the output power of each electric motor is given by the power of the single rotor increased through the Figure of Merit (FOM) to consider the worst conditions. Specifically, the power considered corresponds to the peak reached during the conversion phase from HM to AM (therefore the maximum value obtained in the power profile), reduced for the accessory power. Once the two propulsive branches have been sized, considering the power splitting and knowing that the power of the PGS P_{PGS} equals the power at the beginning of the cruise (including also the accessory power), the power of the batteries is evaluated as:

$$P_{BAT} = 2P_{PROP} - P_{PGS} \tag{5}$$

The knowledge of P_{PGS} allows to size the elements belonging to the PGS branch (from the electrical node to the turboshaft motor), while P_{BAT} allows to size the elements of the battery branch. Note that the value assumed by the P_{BAT} power does not coincide with the power delivered by the batteries, as to get to this, it is necessary to pass through the DC/DC converter and the two circuit breakers present on the considered branch.

3.2 Batteries sizing

The batteries are sized both in terms of power and energy, then choosing the maximum mass value obtained as indicated by the following expression:

$$M_{BAT} = \max\{M^{E}_{BAT}, M^{P}_{BAT}\} \tag{6}$$

where

$$M^{E}_{BAT} = E_{BAT}/e_{BAT} \qquad \textit{and} \qquad M^{P}_{BAT} = P_{BAT}/p_{BAT} \tag{7}$$

with p_{BAT}, e_{BAT} the specific power and energy of the batteries at system level.
In this work, four types of batteries are considered: lithium ion (LiB), lithium sulfur (LiS), lithium air (LiO_2) and lithium polymer (Li-po).Table 3 presents the current values of specific power and energy (2020/2021) in terms of both current. Table 4 report the values estimated for the year 2035 as reported in [1].

Table 3 – Battery parameters with current technology (2020/2021)

Battery type	Specific Power [W/kg]	Specific Energy [Wh/kg]
Lithium Ion	1365 [26]	210 [26]
Lithium Sulfur	1000 [13]	650 [13]
Lithium Air	1000 [13]	610 [26]
Lithium Polymers	5860 [1]	120.2 [1]

Table 4 – Battery parameters with future technology (2035)

Specific Power [W/kg]	Specific Energy [Wh/kg]
19000 [1]	1021.5 [1]

With the current technology, Li-po batteries are the most convenient in terms of weight, corresponding to 1460.49 kg (to comply with the most stringent energy requirement). However, the mass of the

Elements	Mass [kg]
Engine installation	492.2
Air induction	7.7
Exhaust system	7.7
Lubrication system	10
Fuel system	87.1
Engine controls	18.6
Starting system	43.5
Gearboxes	445.9
Interconnect drive	23.6
Total Subtracted Mass	1136.3

Table 5 – Subtracted masses (data from [17])

batteries would already exceed the Subtracted Mass (SM) of 1136.3 kg, which represents the total mass of the elements removed from the original configuration of the XV-15 (see Table 5)
To reduce the weight of the batteries, a new design exploiting a double battery pack, one consisting of Li-po batteries and the other one of LiB batteries (see fig. 5), is proposed. This solution is driven by the following observations: (1) Li-po batteries can be used to cover power peaks, as they are the lightest in the case of power-based sizing; (2) LiB batteries, on the other hand, can be used for the prolonged phase of lower power request as they are the lightest in the case of energy-based sizing; (3) LiS and LiO_2 are excluded due to the fact that these batteries are currently at a lower technological level than LiB.

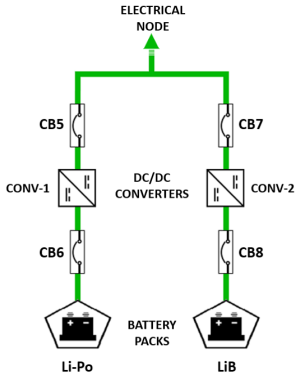

Figure 5 – Double battery branch scheme

With this solution, both power and total energy are split between the two battery packs, with the optimal split shown in fig. 6. Such a design allows to obtain a weight for the Li-po and LiB batteries equal to 670.13 kg and 453.2 kg, respectively, for a total weight of 1122.44 kg, which compared with the weight obtained for Li-po batteries alone leads to a 23.14% weight reduction, resulting in a saving of 141.79 kg. Figure 7 summarizes this result.

However, the weight of the batteries is only slightly lower than that of the SM (by only 13.86 kg). So even in this case, the subtracted masses are almost completely recovered with the mass of batteries alone. Considering the future technology level hypothesized in [1], the overall batteries weight drops to 171.83 kg, with a consistent saving (about 1 ton).

3.3 TMS sizing

Another element to be sized, not part of the propulsion system but still strictly necessary, is the Thermal Management System (TMS) which cools down the propulsive system elements.
A detailed sizing of the TMS is very complex, as it is linked to the type of elements making up the propulsion system, and it affects not only the weight of the aircraft but also its aerodynamics, for example due to the presence of air heat exchangers that require appropriate intakes. Furthermore, to

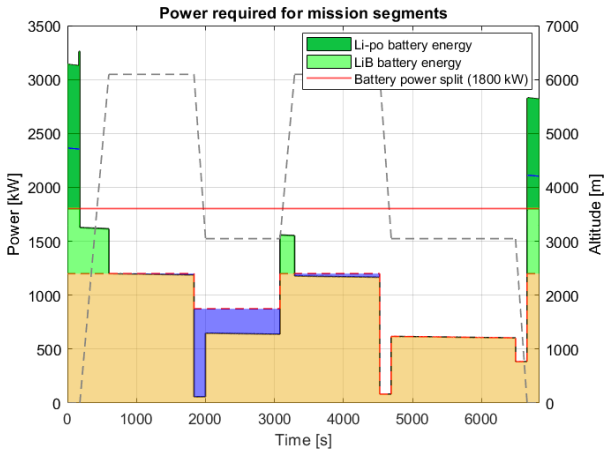

Figure 6 – Double battery optimized power and energy split

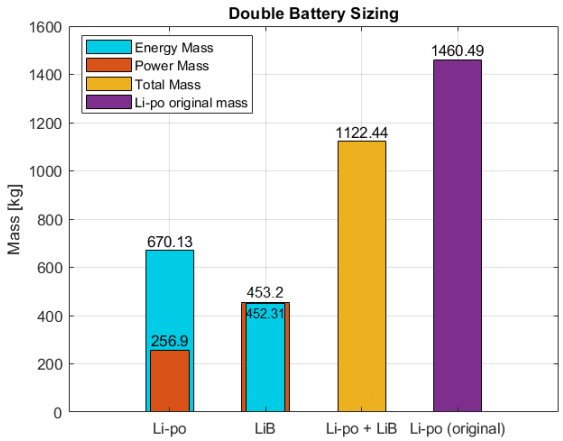

Figure 7 – Comparison between single and double battery weight

the authors' knowledge, no simple models to estimate the power required from the TMS are available in the literature. Following Ref. [35], a rough estimation of the TMS weight is provided, by using the specific power value considered valid for several electric aircraft (MEA) and therefore assumed valid also for this work, corresponding to $p_{TMS} = 0.68\,kW_{th}/kg$. The evaluation of p_{TMS} requires the knowledge of the thermal power developed by the propulsion system. This power is estimated considering that the power lost in heat can be computed from the efficiency and input power of each element of the propulsive system. When High Temperature Superconductors (HTS) are used in place of metallic cables, it is also necessary to estimate the weight of the cryogenic cooler for which the weight can be estimated following the suggestions contained in [21] (see fig. 8).

3.4 Fuel mass evaluation

The fuel required for the mission is evaluated by adding the contributions of fuel burned in each single mission segment. They are obtained as the time integral of the product between each mission segment SFC and power.

Note that the fuel masses used in the sizing process are congruent only if the MTOMs of the hybrid electric XV-15 would result equal to the original DTOM value, which has been used for the calculation of the necessary power of each mission leg.

3.5 Overall weight estimation

Reference [18] provides an overall empty mass (including liquids except fuel) of 4631 kg. It is then possible to proceed with the definition of the new Partial Empty Mass (PEM) of the hybrid electric version of the XV-15 (in the following indicated as HE XV-15) as the difference between the overall empty mass and subtracted mass (3432.7 kg). Once the PEM has been defined, the next step is

the evaluation of the new Propulsion System Mass (PSM) for which the following considerations are made:

- The masses of the propulsion system will be distinguished between current and future battery technology. With regard to current technology, double battery branch configuration is used, while for future technology the minimum mass of the batteries obtained with the single battery branch approach is sufficient, and only Li-po batteries are considered.
- Three cases are distinguished for the cabling system: copper cables, aluminum cables (both characterized by the same TMS) and the third case considering the HTS cables with the relative TMS (which also includes the cryogenic cooling system).

Following a classic approach, the preliminary sizing can be defined with the following expression:

$$\mathrm{MTOM_{new}} = \mathrm{PEM} + \mathrm{PSM} + \mathrm{M_{fuel}} + \mathrm{M_{payload}} + \mathrm{M_{crew}} \tag{8}$$

Where, apart from the PEM and the PSM already defined, the other masses will be considered as follows:

- For the crew, consisting of two pilots, reference [18] gives the indication of 90 kg for each of them.
- For the payload, again reference [18] provides the indication of 407 kg consisting mainly of research instrumentation.

The result for the new MTOM of the aircraft is shown in fig. 8. The difference in mass relating to

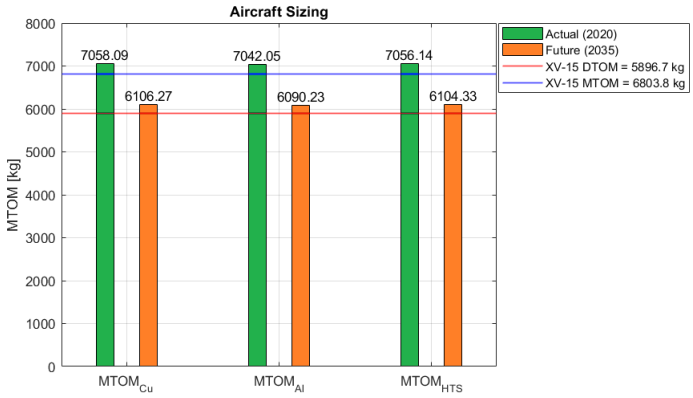

Figure 8 – MTOM after retrofit

the wiring systems is very small, with maximum variations of about 1%. Concerning the difference related to the technological levels of the batteries, an average reduction of 13% can be achieved passing from the current technology to the hypothesized future one.

Finally, it is important to note that all the overall masses obtained with the current technology are higher than the original value of the Design Take Off Mass of the XV-15 (red horizontal line in the figure) and Maximum Take Off Mass (blue horizontal line in the figure). Considering the 2035 technology level, the weight of the retrofit XV-15 would drop below original MTOM, but would remain higher than original DTOM.

4. Emergency landing modelling

This section addresses safety issues related to the hybrid electric version of the XV-15 and defines an emergency landing procedure. The most critical condition for an engine failure to occur has been considered as the beginning of the first cruise segment, when the batteries are at their minimum state of charge after the previous power-intensive phases of vertical take-off, conversion, and climb. Therefore, in the hypothesis of a failure of the turboshaft engine at the end of the climb, the aircraft

would find itself without propulsive power during the descent and, more importantly, at landing or in helicopter mode.Landing in helicopter mode is critical provided that (i) some residual energy is required for tilting the nacelles upwards, (ii) the final approach should be performed after transitioning from a fixed-wing gliding flight to an autorotation mode (a maneuver far from trivial, although already performed [33]), (iii) the touch-down in autorotation still requires a considerable amount of obstacle-free space, provided the rotational kinetic energy of the prop-rotors is unlikely to be sufficient for fully stopping the vehicle prior to touchdown, and, finally, (iv) landing in autorotation is even more difficult for a tiltrotor than for a conventional helicopter, due to the reduced aerodynamic performance.
The development of an appropriate emergency landing procedure is thus a relevant issue for the overall safety of the vehicle. The idea at the basis of this procedure is to recharge the batteries with an amount of energy sufficient for performing a short electrically powered vertical emergency landing. Batteries are recharged assuming that electric motors can be used as generators, receiving mechanical power from the rotors used as the prime mover, in a windmilling condition. Thus, the glide descent performed in aircraft mode is also intended as a regenerative descent and braking phase, transforming part of the potential and kinetic energy of the tiltrotor at the moment of the engine failure into chemical energy stored in the batteries.
The procedure is divided into a sequence of four steps (see Figure 9):

1. gliding flight from cruising altitude (assumed equal to 20000 ft), at which the failure occurs, down to an altitude of approximately 1000 ft above sea level, during which the batteries are recharged;
2. conversion from Aircraft Mode (AM) to Helicopter Mode (HM), which takes approximately 12 s, around an altitude of 1000 ft;
3. autorotation for approximately 2/3 of the remaining altitude after conversion (650 ft, that is, 200 m);
4. use of the energy stored in the batteries for a powered 350 ft (approximately 100 m) descent and a short hover phase for a safe vertical landing.

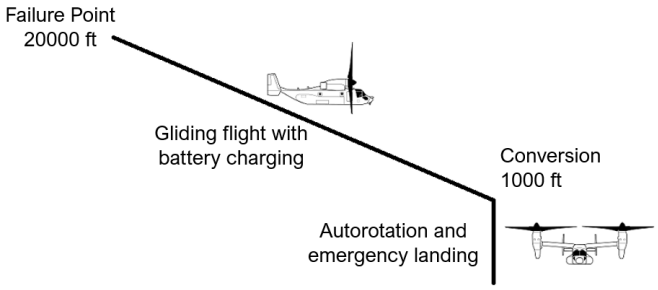

Figure 9 – Emergency procedure

4.1 Application of Betz theory for rotor in windmilling conditions

The regenerative process used for battery recharge during the glide is analyzed on the basis of the classic Betz theory for wind turbines [2]. Applying Bernoulli's theorem and mass and momentum conservation laws as described in [12], one obtains that the power extracted from the relative wind and the thrust (positive in the flow direction) generated by the rotor are equal to, respectively,

$$P_e = \frac{1}{2}\rho A V^3 4a(1-a)^2 \tag{9}$$

$$T = \frac{1}{2}\rho A V^2 4a(1-a) \tag{10}$$

where A is the area of the rotor disk, V is the speed of the free-stream, and a is the interference factor, such that

$$u = (1-a)V \tag{11}$$

with u equal to the flow velocity at the rotor disc, which can be shown to be given by the arithmetic mean between V and the flow velocity in the wake downstream of the rotor disc [12]. Differentiating the expression above, one obtains the Betz's limit which implies that at most only 59% of the power of the flow passing through the rotor disk can be converted into mechanical power at rotor shaft [12]. Moreover, this is a purely theoretical limit, since viscous effects and 3-D features of the flow field further reduce the actual power generated by a wind turbine to a fraction of this value (up to 80% for most efficient wind turbines). Moreover, assumptions at the basis of Betz's theory are valid for values of a less than 0.4, approximately [8].

4.2 Blade element theory corrections to power balance

To derive a more reliable power balance, some corrections to the expression of rotor power and thrust derived in the framework of Betz's theory are introduced. Specifically, two contributions to energy dissipation are considered. The first is associated with the component of friction drag ΔD_r acting on rotor blades in the direction opposite to the aircraft motion, whereas the second one, $P_0^w = -Q_D\Omega$, referred to as profile power in windmilling condition, is associated with the in-plane blade drag component, which produces a net torque Q_D against rotor rotation Ω. These contributions are evaluated using the blade element theory [16].

4.3 Power balance in gliding flight

The power balance equation during gliding flight can be written in the form

$$mg\dot{h} + mV\dot{V} = -\left(DV + D_rV\right) \tag{12}$$

where the meaning of the different terms is reported below.

- The first term on the left-hand side represents the potential energy derivative with respect to time.
- The second term on the left-hand side represents the derivative of the vehicle kinetic energy with respect to time.
- The first term on the right-hand side represents the parasite power of the aircraft, expressed as usual by the product of aerodynamic drag times forward speed:

$$DV = \frac{1}{2}\rho V^3 S C_D \tag{13}$$

  where the drag coefficient C_D is the sum of parasite drag coefficient C_{D_0} and induced drag kC_L^2, with k the induced drag factor. As a consequence, at gliding equilibrium C_D depends on aircraft weight, that is,

$$DV = \frac{1}{2}\rho V^3 S\left[C_{D_0} + k\left(\frac{2W}{\rho V^2 S}\right)^2\right] \tag{14}$$

- Finally, the second term on the right-hand side represents the power associated with forces generated by the rotors in windmilling conditions, hence related to power generation, as stated by Betz's theory. Rather than being a propulsive force, D_r acts in a direction opposite to the aircraft motion, thus representing an additional drag term given by $D_r = 2T + \Delta D_r$ to account for the contribution of both rotors (see Eq.(10)) and the drag of all the blades (ΔD_r).

4.4 Evaluation of total energy recovered

The contribution of T to D_r in eq. (12) causes the power balance to depend on the interference factor, a. Combining the equation for D_r with Equations (10) and (14), the power balance can be rewritten as a quadratic equation in a:

$$a^2 - a - \frac{mg\dot{h}}{4\rho V^3 A} - \frac{mV\dot{V}}{4\rho V^3 A} - \frac{S}{8A}\left[C_{D_0} + K\left(\frac{2W}{\rho S V^2}\right)^2 + \Delta C_{Dr}\right] = 0 \tag{15}$$

where $\Delta C_{Dr} = \Delta D_r / \left(\frac{1}{2}\rho V^2 S\right)$.
Equation (15) has in general two roots, but only those lying in the range $0 < a < 0.4$ are acceptable, due to the limits for an equilibrium in windmilling condition ($a > 0$) and Betz's theory validity ($a < 0.4$). Once a prescribed variation for the deceleration profile $\dot{V}(t)$ is assumed and the corresponding descent/deceleration time t_f is assigned, eq. (15) can be solved with respect to a at any time instant in the interval $0 < t < t_f$, which is the total glide time interval. Once the interference factor a is determined, eq. (9) allows evaluating the instantaneous ideal value of the power $P_e(t)$ extracted from the current.
The instantaneous power recharging the batteries is thus expressed as

$$P_e(t) = \eta_{tot}\left\{\left[\frac{1}{2}\rho A V^3 4a(1-a)^2\right] - P_o^{\omega}\right\} \tag{16}$$

where η_{tot} is the overall electric efficiency, considering generator, energy converter, cables, safety circuit breakers and batteries, and P_o^{ω} is the rotor parasite power.
Finally, the total extracted energy E_e is calculated by integrating it during the glide segment:

$$E_e = \int_0^{t_f} P_e(t)dt \tag{17}$$

A limit is enforced on maximum power that can be generated from each electric motor (which in this case operates as a generator), assuming it is equal to the maximum power that can be supplied by the electric motor in its normal operating mode. Similarly, all the cases in which an instantaneous negative power is obtained after subtracting drag losses are discarded too, since this would decrease rotor kinetic energy. Finally, all the cases that result in a regenerated energy smaller than 20 kWh has been discarded in order to guarantee a sufficient hovering time.

5. Emergency landing analysis

The emergency landing procedure is tested for a cubic deceleration law between initial V_i and final velocities V_f, namely the cruise and the conversion ones, with final time t_f and initial deceleration $\dot{V}_i$ as parameters

$$V_{cub}(t) = V_i + (V_f - V_i)[3(t/t_f)^2 - 2(t/t_f)^3] + \dot{V}_i t[1-(t/t_f)]^2$$

The final deceleration has been set to zero in order to guarantee a smooth transition to conversion phase. The rate of descent between initial altitude h_i =20000 ft and final altitude h_i =19000 ft has been hypothesized to vary linearly along the maneuver.

$$\dot{h}(t) = \dot{h}_i + (\dot{h}_f - \dot{h}_i)(t/t_f)$$

The value of $\dot{h}_f = -14$ m/s is equal for all the considered cases, and it corresponds to a final descent angle γ_f slightly above -21 deg, which represents a rather steep descent at which a flare for a conversion to helicopter mode can be started. The initial value, $\dot{h}_i$, is evaluated in such a way that the total altitude lost during the glide is equal to $\Delta h = (\dot{h}_i + \dot{h}_f)(t_f/2) = 19\ 000$ ft. Hence, $\dot{h}_i$ depends uniquely on t_f, when $\dot{h}_f$ is prescribed.
Figure 10 summarizes the active constraints in the design space identified by descent time and initial deceleration, as well as the resulting admissible subspace, where the regenerated energy is shown by means of a colored contour plot. The admissible area is roughly triangular. The lower boundary is represented by the constraint on maximum generated power, whereas the remaining bounds are defined by the minimum power and minimum energy (in the upper corner) constraints. Finally, a constraint on the maximum descent angle is also introduced (cyan line), which rules out the region where descent angles overcome 40 deg at some point during the maneuver. Reducing the value of the constraint to smaller values of the maximum descent angle would further reduce the admissible region. Also in this case, the maximum power constraints is more stringent than that on the interference factor, suggesting that the choice of a different rotor drive would allow for a higher value of regenerated power.
Physically acceptable results are obtained for a range of initial deceleration $\dot{V}_i \in [-2., 0.]$ m/s^2, at the bottom of the feasible region, for smaller glide times. The feasible region gets narrower for longer

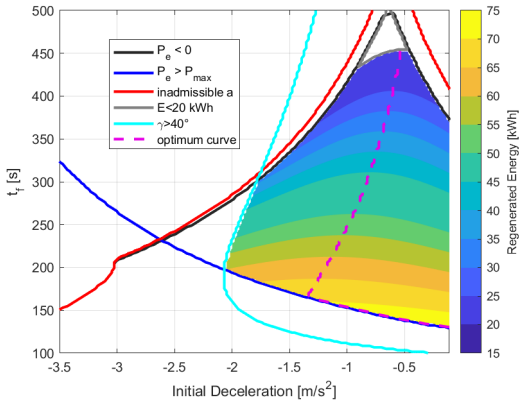

Figure 10 – Regenerated energy in the design space for the cubic speed law.

glide times, with a regular trend of the regenerated energy, E_e. A relative maximum of E_e for each value of t_f is obtained at approximately half of the range of admissible initial deceleration values for $t_f > 165$ s, whereas for $130 \leq t_f \leq 165$ s the maximum of E_e is on the bottom bound of the admissible region. In the figure, the purple dashed line identifies the optimal value of $\dot{V}_i$ for a given t_f. The values of the relative maxima of E_e as a function of t_f are instead depicted in Figure 11 (which also shows the corresponding value of available hover time at the end of the glide, after conversion). Extracted energy and hovering time achieves a maximum value of 74.5 kWh and 110 s respectively (slightly above the value obtained with linear and quadratic speed laws) for $t_f = 150$ s and an initial deceleration close to 0 $\mathrm{m/s^2}$, in the bottom right corner of the feasible region of the contour plot. For higher values of t_f, an almost linear monotonic decrease of regenerated energy is obtained, with the optimum $\dot{V}_i$ initially following the bottom constraint on maximum power, up to 165 s, where $\dot{V}_i = -1.35$ m/s^2. For increasing values of t_f the optimal value of $\dot{V}_i$ decreases in absolute value towards $\dot{V}_i = -0.55$ m/s^2 for the longest glide, with $t_f = 455$ s.

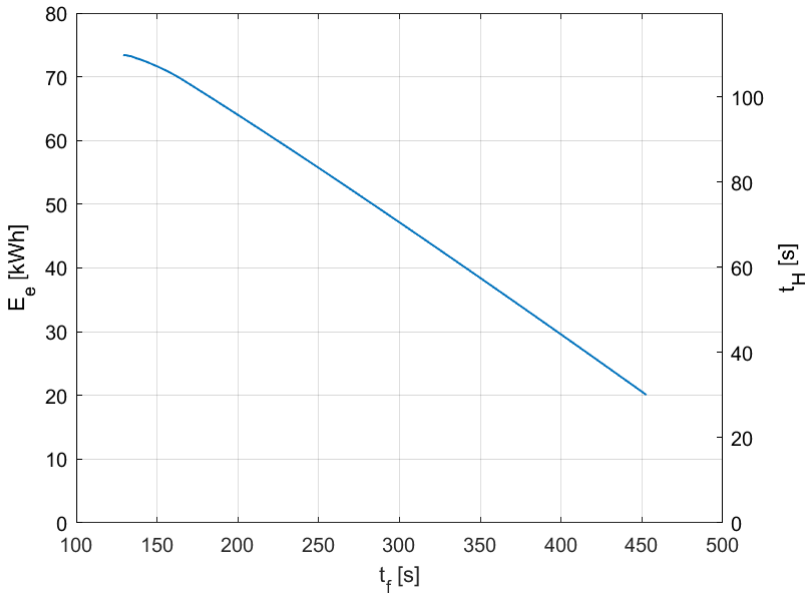

Figure 11 – Maximum regenerated energy as a function of descent time, cubic speed law.

The role of the initial deceleration, $\dot{V}_i$, is relevant, since it represents a degree of freedom in the choice of the descent strategy left to the pilot after the initial decision, allowing a trade-off between hovering time and distance traveled during the descent, shown in fig. 12. Indeed, long descent time and low initial deceleration provide the longest glides but lower regenerated energy and thus to the shorter hovering time.

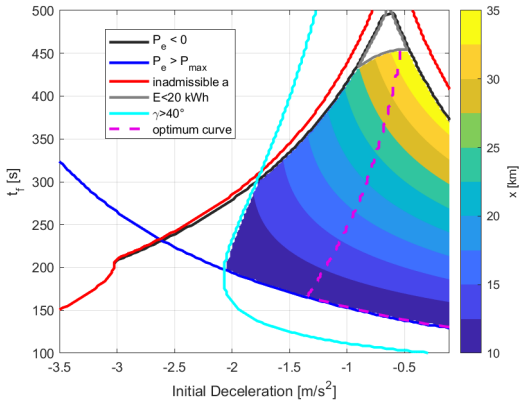

Figure 12 – Distance traveled during the descent.

6. Conclusions

The retrofit process of the XV-15 to a series-hybrid powertrain has demonstrated that the current technological level of batteries is not sufficient, in terms of specific energy and power, to have an electrified version of the XV-15 with the same weight. However, two additional considerations must be done. The batteries performance has constantly improved during last years with a significant rate, which would allow a feasible retrofit in less than 20 years. Moreover, the electrification of a tiltrotor allows a significant improvement in the wing performance and weight, which makes the weight parity closer. This needs to be quantified in a complete design process. The emergency management of a hybrid tiltrotor in case of the turboshaft failure is greatly simplified by the presence of batteries. However, also in the case of depleted batteries at the moment of the failure, the authors demonstrated that the tiltrotor gliding may be used as a regenerative phase, in order to allow a powered landing in helicopter mode. The best trade-off between the opposed goals of traveled distance during the gliding phase and regenerated energy can be chosen by the pilot as a function of landing constraints.

7. Copyright Statement

References

[1] G. Avanzini, A. Carlà, and T. Donateo. Parametric analysis of a hybrid power system for rotorcraft emergency landing sequence. *Proceedings of the institution of mechanical engineers, part G: journal of aerospace engineering*, 231(12):2282–2294, 2017.

[2] A. Betz. *Introduction to the theory of flow machines*. Elsevier, 1966.

[3] A. Bills, S. Sripad, W. L. Fredericks, M. Singh, and V. Viswanathan. Performance metrics required of next-generation batteries to electrify commercial aircraft. *ACS Energy Letters*, 5(2):663–668, 2020.

[4] J. J. Botti. Hybrid electric aircraft to improve environmental impacts of general aviation. *The Bridge*, 50(2), 2020.

[5] W. W. Chung, D. Linse, A. Paris, D. Salvano, T. Trept, T. Wood, H. Gao, D. Miller, K. Wright, R. Young, et al. *Modeling High-speed Civil Tiltrotor Transportgs in the Next Generation Airspace*. National Aeronautics and Space Administration Ames Research Center, 2011.

[6] R. A. Danis, M. W. Green, J. L. Freeman, and D. W. Hall. Examining the conceptual design process for future hybrid-electric rotorcraft. Technical Report CR—2018–219897, NASA, 2018.

[7] D. C. Dugan, R. G. Erhart, and L. G. Schroers. *The XV-15 tilt rotor research aircraft*. NASA, 1980.

[8] D. M. Eggleston and F. Stoddard. *Wind turbine engineering design*. Van Nostrand Reinhold Co. Inc., New York, NY, 1987.

[9] A. Eppinga. Future of electric aviation: 'batteries only suitable for small-scale

flights'. *Innovation Origins*, August 2021. https://innovationorigins.com/en/future-of-electric-aviation-battery-only-suitable-for-small-scale-flights/.

[10] R. Furchgott. Can hydrogen save aviation's fuel challenges? it's got a way to go. *New York Times*, November 2021. https://www.nytimes.com/2021/11/15/business/airplanes-hydrogen-fuel-travel.html.

[11] K. Hamilton and T. Ma. Electric aviation could be closer than you think. *Scientific American*, November 2020. https://www.scientificamerican.com/article/electric-aviation-could-be-closer-than-you-think/.

[12] M. Hansen. *Aerodynamics of wind turbines*. Routledge, 2015.

[13] J. Hoelzen, Y. Liu, B. Bensmann, C. Winnefeld, A. Elham, J. Friedrichs, and R. Hanke-Rauschenbach. Conceptual design of operation strategies for hybrid electric aircraft. *Energies*, 11(1):217, 2018.

[14] I. F. Kuhn Jr. Purebred and hybrid electric vtol tilt rotor aircraft, June 25 2013. US Patent 8,469,306.

[15] S. Kulandaivalu and Y. Sulaiman. Recent advances in layer-by-layer assembled conducting polymer based composites for supercapacitors. *Energies*, 12(11):2107, 2019.

[16] G. J. Leishman. *Principles of helicopter aerodynamics with CD extra*. Cambridge university press, 2006.

[17] J. Magee and H. Alexander. ì a hingeless rotor xv-15 design integration feasibility study, volume i and ii. Technical report, î NASA-CR-152310, 1978.

[18] M. D. Maisel. NASA/Army XV-15 tilt rotor research aircraft familiarization document. Technical Report TM-X62, Ames Research Center, NASA, 1975.

[19] S. Morris. 'decarbonising aviation': the electric EEL could be the future of flying. *The Guardian*, August 2021. https://www.theguardian.com/environment/2021/aug/24/decarbonising-aviation-the-electric-eel-could-be-the-future-of-flying.

[20] A. Narishkin, E. Ocbazghi, and S. Cameron. Why electric planes haven't taken off yet. *Business Insider*, April 2021. https://www.businessinsider.com/electric-planes-future-of-aviation-problems-regulations-2020-3?r=US&IR=T.

[21] R. Radebaugh. Cryocoolers for aircraft superconducting generators and motors. In *AIP Conference Proceedings*, volume 1434, pages 171–182. American Institute of Physics, 2012.

[22] M. A. Rendón, J. Gallo, A. H. Anzai, et al. Aircraft hybrid-electric propulsion: Development trends, challenges and opportunities. *Journal of Control, Automation and Electrical Systems*, pages 1–25, 2021.

[23] J.-P. Rodrigue. *The geography of transport systems*. Routledge, 2020.

[24] S. Rondinelli, R. Sabatini, A. Gardi, et al. Challenges and benefits offered by liquid hydrogen fuels in commercial aviation. In *Practical Responses to Climate Change Conference 2014*, pages 216–226. Engineers Australia Barton, ACT, 2014.

[25] N. Rufford. Are electric planes the future of flight? *The Times*, November 2021. https://www.thetimes.co.uk/article/are-electric-planes-the-future-of-flight-mvr738dn0.

[26] F. Salucci. *Design of electric-powered aircraft for commercial transportation*. PhD thesis, Polytechnic of Milan, 2021.

[27] J. Serafini, M. Cremaschini, G. Bernardini, L. Solero, C. Ficuciello, and M. Gennaretti. Conceptual all-electric retrofit of helicopters: Review, technological outlook, and a sample design. *IEEE Transactions on Transportation Electrification*, 5(3):782–794, 2019.

[28] F. Stagliano and M. Hornung. Impact of novel propulsion system architectures incorporating diesel engines on mission fuel burn for a tilt-wing transport aircraft. In *12th AIAA Aviation Technology, Integration, and Operations (ATIO) Conference and 14th AIAA/ISSMO Multidisciplinary Analysis and Optimization Conference*, page 5587, 2012.

[29] P. C. Vratny, H. Kuhn, and M. Hornung. Influences of voltage variations on electric power architectures for hybrid electric aircraft. *CEAS Aeronautical Journal*, 8(1):31–43, 2017.

[30] VV.AA. E-fan x - a giant leap towards zero-emission flight. https://www.airbus.com/en/innovation/zero-emission/electric-flight/e-fan-x.

[31] VV.AA. Electric and hybrid aircraft platform for innovation (e-hapi). https://www.icao.int/environmental-protection/Pages/electric-aircraft.aspx.

[32] VV.AA. Electric flight - laying the groundwork for zero-emission aviation. https://www.airbus.com/en/innovation/zero-emission/electric-flight.

[33] VV.AA. Aw1152 aw609 autorotation trials completion, April 2014. https://www.leonardo.com/en/press-release-detail/-/detail//aw609-autorotation-trials-completion.

[34] VV.AA. Notice of proposed amendment 2016-06 (B) - fuel planning and management. Technical report, EASA, 2016.

[35] J. Welstead and J. L. Felder. Conceptual design of a single-aisle turboelectric commercial transport with fuselage boundary layer ingestion. In *54th AIAA aerospace sciences meeting*, page 1027, 2016.

[36] X.-G. Yang, T. Liu, S. Ge, E. Rountree, and C.-Y. Wang. Challenges and key requirements of batteries for electric vertical takeoff and landing aircraft. *Joule*, 2021.

[37] L. Young, W. Chung, A. Paris, D. Salvano, R. Young, H. Gao, V. Cheng, and K. Wright. Civil tiltrotor aircraft operations. In *11th AIAA Aviation Technology, Integration, and Operations (ATIO) Conference, including the AIAA Balloon Systems Conference and 19th AIAA Lighter-Than*, page 6898, 2011.

[38] J. Zamboni, R. Vos, M. Emeneth, and A. Schneegans. A method for the conceptual design of hybrid electric aircraft. In *AIAA Scitech 2019 Forum*, 2019.

[39] F. Zhang and J. Maddy. Investigation of the Challenges and Issues of Hydrogen and Hydrogen Fuel Cell Applications in Aviation. `https://www.techrxiv.org/articles/preprint/Investigation_of_the_Challenges_and_Issues_of_Hydrogen_and_Hydrogen_Fuel_Cell_Applications_in_Aviation/14958057`, 7 2021.

[40] J. F. Zugschwert, J. Leverton, R. R. Wilkins, S. Charles, and R. Reber. Tiltrotor and advanced rotorcraft technology in the national airspace system (tartnas). Technical report, FAA RE&D Committee Vertical Flight Subcommittee, 2001.